Encircling exceptional points in non-Hermitian systems with quasidegenerate energy levels

Ming-Xuan Shi,[1] X. M. Su,[1] and Xu-Lin Zhang[2,*]
[1]*College of Physics, Jilin University, Changchun 130012, China*
[2]*State Key Laboratory of Integrated Optoelectronics, College of Electronic Science and Engineering, Jilin University, Changchun 130012, China*

(Received 18 February 2022; revised 27 May 2022; accepted 15 June 2022; published 27 June 2022)

Dynamically encircling an exceptional point in non-Hermitian systems shows a chiral state switching behavior as a result of the nonadiabatic transition between nonorthogonal eigenstates. It has been revealed that the chiral dynamics is protected by the topological structure of eigenvalue sheets where only one lowest-loss sheet exists. This raises the question on what the dynamics would be in non-Hermitian systems possessing multiple degenerate lowest-loss energy levels. Here, we address this question by studying a photonic-waveguide-array non-Hermitian system where two exceptional points are encircled dynamically. The system possesses four quasidegenerate lowest-loss eigenvalue sheets and such topological structure results in an exotic nonchiral behavior for switching eigenstates such that the final state is always a superposition of the four lowest-loss eigenstates. We find that this intriguing phenomenon is robust to a certain perturbation of the system parameters. Our findings enrich the understanding of exceptional point-encirclement physics and may inspire potential non-Hermitian applications for manipulating waves.

DOI: 10.1103/PhysRevA.105.062214

I. INTRODUCTION

Open systems governed by non-Hermitian Hamiltonians which extend the Hermiticity postulate and break conservation of energy induced by gain and loss, exhibit distinctive singularities that are called exceptional points (EPs) [1–5], at which the eigenvalues and the corresponding eigenvectors coalesce simultaneously. The existence of EPs has been realized, and relevant implementations have brought fruitful works in various platforms including magnon polaritons [6–8] in magnomechanics, acoustic cavities [9,10] or leaky waveguides [11] in acoustics and especially coupled atom cavities [12], optical microresonators [13–20] and coupled optical waveguides [21–29] in optics. In addition, a series of applications associated with EPs in parity-time ($\mathcal{PT}$) symmetric systems such as enhanced sensing [15,18,30,31], topological photonics [32–36], unidirectional invisibility [37–40], induced transparency [19,41,42], coherent perfect absorption [43–46] and laser physics [13,16,20,47–49], have made further progress over the past decade. An interesting feature of the non-Hermitian system is its topological structure, which is defined as the intersecting eigenvalue sheets around the EPs in a parameter space. A remarkable phenomenon related to the topological structure is the state switching when the EPs are dynamically encircled [21–28,50–54]. In this process, a state evolving on the eigenvalue sheets can experience nonadiabatic transitions (NATs) due to the nonorthogonality of the eigenstates in non-Hermitian systems [2,5,55]. The occurrence of NATs is fundamentally related to the Stokes phenomena of asymptotics [55], and accompanied by the nonadiabatic coupling between different eigenstates which can be exponentially amplified, leading to a selective final state, which is usually the one with lowest-loss [51,56]. As a result, the NATs as well as the topological structure around the EPs give rise to a chiral state switching behavior, i.e., the final state is irrelevant to the initial state, but solely depends on the encircling direction [50–52,55,56]. This intriguing phenomenon has been demonstrated and verified in a variety of experiments [21–28,52]. Although a general rule governed the EP encirclement process has been proposed for periodic systems [28], all previous studies focus on non-Hermitian systems with only one energy level having the lowest loss. In this case, only the NAT towards this lowest-loss sheet can occur, resulting in the fact that the final state is a single eigenstate located on this sheet. However, what happens to non-Hermitian systems with multiple degenerate lowest-loss energy levels? This is still an open question since the NAT has multiple targets, and the dynamics would be quite different from that in the system possessing only one lowest-loss energy level.

In this paper, we address the above question by investigating a waveguide-based non-Hermitian system with multiple quasidegenerate lowest-loss eigenvalue sheets and revealing the physical consequence in the process of dynamical encircling of the EPs. We establish a non-Hermitian Hamiltonian to capture the physics of the system and calculate the output field distribution by solving the Schrödinger-like equation. We discover an exotic nonchiral feature by encircling the EPs, which is distinct from the acquainted chiral dynamics. Whatever the input state is and whichever the encircling direction is, the final state is always a superposition of multiple quasidegenerate eigenstates with lowest loss. The nonchiral dynamics is protected by the topological structure of eigenvalue sheets so that it is robust to system perturbations such as the device

*Corresponding author: xulin_zhang@jlu.edu.cn

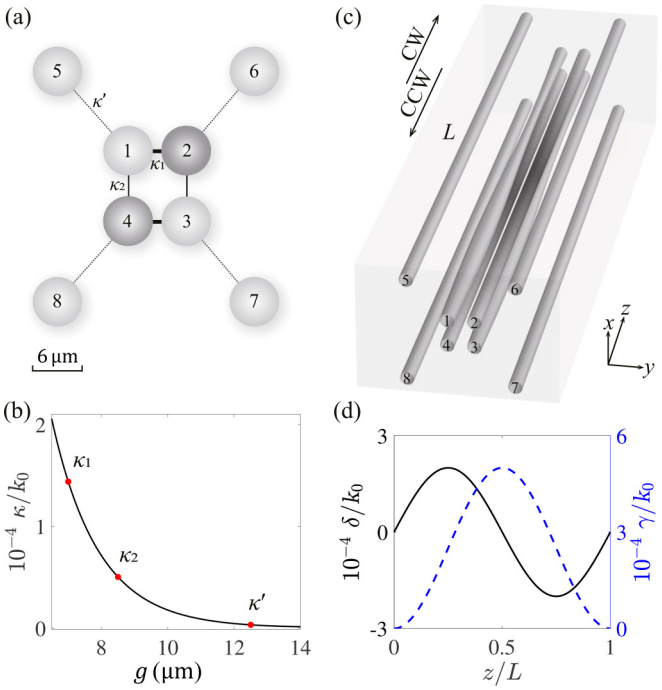

FIG. 1. (a) Cross-section view of the non-Hermitian system under study which consists of eight waveguides. (b) Coupling coefficient κ as a fitting function of the gap distance g between adjacent waveguides. The three red circles mark the values of κ_1, κ_2, and κ' defined in (a), corresponding to gap distances of $g_1 = 7$ μm, $g_2 = 8.5$ μm and $g' = 12.5$ μm. (c) Schematic diagram of the non-Hermitian waveguide arrays, where waveguides 2 and 4 exhibit a position-dependent losses while waveguides 1 and 3 have a position-dependent propagation constant. (d) The variation of $\delta(z)$ and $\gamma(z)$ along the waveguiding direction.

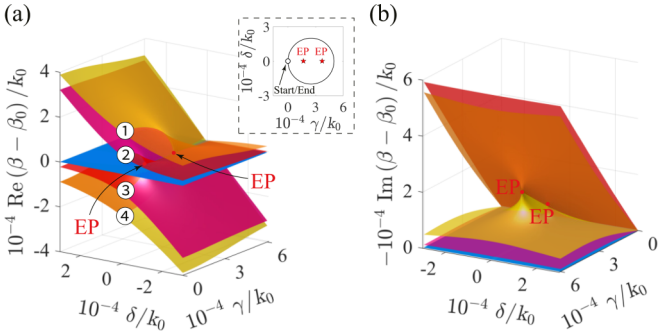

FIG. 2. Calculated real part (a) and imaginary part (b) of the eigenvalues of the non-Hermitian system in the $\delta-\gamma$ parameter space, where the blue sheet represents four quasidegenerate eigenstates exhibiting the lowest loss. The inset of (a) shows the position of the two EPs and the ellipse encircling loop in the parameter space.

length and the form of the encircling loop. Finally, we discuss the difference between the nonchiral and chiral characteristics in the EP encirclement process.

II. NONCHIRAL DYNAMICS IN SYSTEMS WITH QUASIDEGENERATE ENERGY LEVELS

The system under study is a photonic waveguide array consisting of eight waveguides. Figure 1(a) illustrates the cross section of the waveguide array. The waveguides 2 and 4 are lossy while the other waveguides are lossless with a refractive index of 1.504, while that of the background is set to be 1.5. Each waveguide has a circle cross section with a radius of 3 μm, under which only one eigenmode polarized along the x axis is supported which is the working mode in this work. Such a configuration can be realized in potential experiments by using the femtosecond laser direct writing techniques [28,57,58]. The gap distance g between adjacent waveguides determines the coupling coefficient κ, and their relationship is given in Fig. 1(b). The coupling coefficient between waveguides 1 and 2 (or 3 and 4) is denoted by κ_1, and that between waveguides 1 and 4 (or 2 and 3) is represented by κ_2. The waveguides 1, 2, 3, and 4 are coupled with 5, 6, 7, and 8 respectively, through a coupling coefficient κ'. The values of the three coupling coefficients are marked in Fig. 1(b).

Figure 1(c) shows a three-dimensional schematic diagram of our system, where some structural parameters are changing along the waveguiding direction (i.e., the z axis). To be specific, the cross section size of waveguide 1 (or 3) is nonuniform along the waveguiding direction so that the propagation constant (i.e., the eigenvalue or on-site energy which is denoted by $\beta_{1,3}$) is position-dependent as $\beta_{1,3}(z) = \beta_0 + \delta(z)$, where $\beta_0 = 1.502k_0$ is the propagation constant of a uniform waveguide (e.g., the waveguides 5–8) with k_0 being the wave vector in free space. Therefore, $\delta(z)$ can be considered as a position-dependent detuning parameter. In waveguides 2 and 4, we have introduced position-dependent losses so that their eigenvalues can be written as $\beta_{2,4}(z) = \beta_0 - i\gamma(z)$, where $\gamma(z)$ represents the loss of the mode which can be realized in potential experiment by introducing scatters inside the waveguide [28]. Figure 1(d) plots the variation of $\delta(z)$ and $\gamma(z)$ where the length of the array is L. Here we can also consider them in a $\delta-\gamma$ parameter space in which their variations along the z axis exactly form a closed loop [see the inset of Fig. 2(a)]. The propagation of photonic modes in the waveguides along the $+z$ axis corresponds to the evolution in this parameter space following a clockwise (CW) loop, and vice versa for a counterclockwise (CCW) loop description.

We show that this loop encloses two EPs so that wave propagations in the proposed structure correspond to the dynamical encircling of two EPs in the considered parameter space. To show this point, we solve the eigenvalue of the non-Hermitian system by considering its Hamiltonian

$$H = \begin{pmatrix} H' & D \\ D & 0 \end{pmatrix}, \tag{1}$$

where

$$H' = \begin{pmatrix} \delta & \kappa_1 & 0 & \kappa_2 \\ \kappa_1 & -i\gamma & \kappa_2 & 0 \\ 0 & \kappa_2 & \delta & \kappa_1 \\ \kappa_2 & 0 & \kappa_1 & -i\gamma \end{pmatrix} \tag{2}$$

and

$$D = \begin{pmatrix} \kappa' & 0 & 0 & 0 \\ 0 & \kappa' & 0 & 0 \\ 0 & 0 & \kappa' & 0 \\ 0 & 0 & 0 & \kappa' \end{pmatrix}. \tag{3}$$

In the Hamiltonian, the on-site energy term β_0 is omitted. We then calculate the eigenvalues of the Hamiltonian characterized by the 8×8 matrix in the $\delta - \gamma$ parameter space. The results are shown in Figs. 2(a) (real part) and 2(b) (imaginary part). The blue sheet represents four quasidegenerate eigenstates that share the same lowest-loss, while the other four eigenstates constitute the eigenvalue sheets of pairwise bifurcation which involve two EPs. We choose the point with $\delta = \gamma = 0$ in the parameter space [see the inset of Fig. 2(a)] as the starting point of the loop, where we label the four eigenstates with nonzero losses as eigenmodes 1, 2, 3, and 4, which will be used as the initial states in the following analysis. The positions of the two EPs are shown in the inset of Fig. 2(a), namely at $\gamma = 1.68 \times 10^{-4} k_0$ and $\gamma = 3.71 \times 10^{-4} k_0 (\delta = 0$ for both). The elliptical loop trajectory follows the parametric equations $\delta(z) = 2 \times 10^{-4} k_0 \sin(2\pi z/L)$ and $\gamma(z) = 2.5 \times 10^{-4} k_0 (1 - \cos(2\pi z/L))$, where $z \in [0, L]$ for CW loops and $z \in [L, 0]$ for CCW loops. The field distribution in the evolution process can be simulated by numerical software, but it is too time consuming and impractical. For the sake of simplicity, the overall evolution process can be solved by the Schrödinger-like equation $i\partial_z |\phi(z)\rangle + H(z)|\phi(z)\rangle = 0$, where $|\phi(z)\rangle$ is the instantaneous state vector. The reason why we treat this way is that the waveguide arrays meet the paraxial approximation conditions with a refractive index contraction of $\sim$0.004. Since the amplitude of the state vector is decreased significantly along the waveguiding direction due to the losses in the non-Hermitian system, we introduce a renormalization method for the instantaneous field to improve the readability. Specifically, we denote $|\phi_i|$ (i.e., the magnitude of the ith element of the state vector) as the "instantaneous field" in waveguide $i (i = 1, 2, \ldots, 8)$ and $|\phi|$ as the normalization of the instantaneous state vector. In this way, we will show the ratio $|\phi_i|/|\phi|$ in the following results.

We numerically calculate the evolution of the normalized components of $|\phi(z)\rangle$ in a device following a CW loop, with the eigenmodes 1, 2, 3, and 4 being the initial state, respectively. The device length is set to be $L = 200$ mm. The results are shown in Figs. 3(a)–3(d). In each figure, the input (left panel) and output field distributions (right panel) are also drawn by considering the calculated state vector. Note that at the output side, the phase information is not that important so that it is shown as intensity, distinct from the input field, which contains phase information marked with different colors. We find that encircling two EPs in a CW loop causes the phenomenon that whichever eigenmode the input is, the output state will be approximately evenly distributed in the edge waveguides 5–8. The output field strengths in waveguides 5 and 7 (as well as 6 and 8) are always the same, which is governed by the symmetry of the system. The symmetry lies in the fact that when κ' is significantly smaller than κ_1 and κ_2, the Hamiltonian can be approximately partitioned into two independent components: H' and a 4×4 zero matrix, while

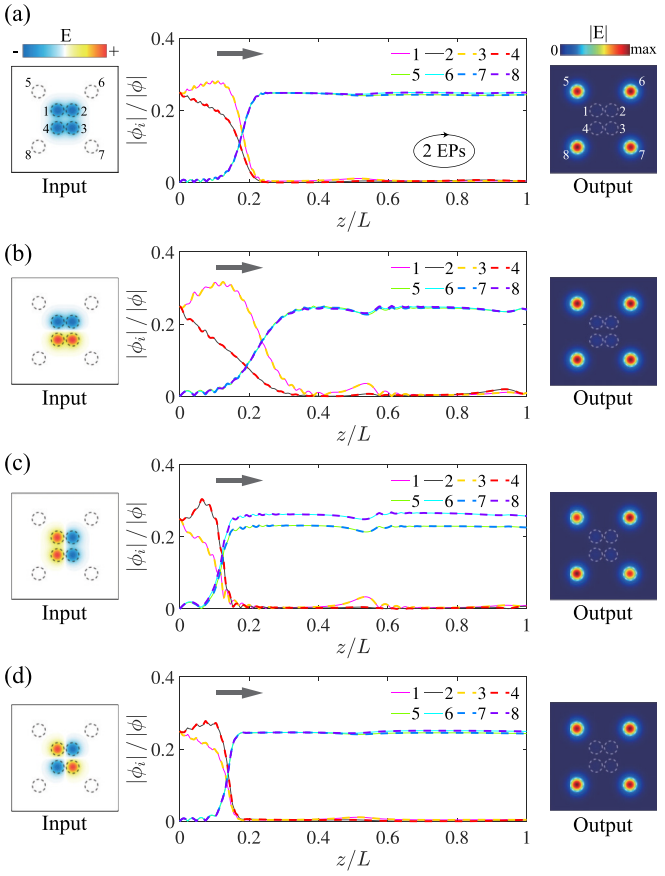

FIG. 3. Numerically simulated evolution of the normalized components of $|\phi(z)\rangle$ (middle) by solving the Schrödinger-like equation in our device with eigenmodes 1 (a), 2 (b), 3 (c), and 4 (d) being the initial state. The left panel and right panel show, respectively, the input (real part of the field) and output (field intensity) field distributions. In the device, two EPs are dynamically encircled in a CW direction which corresponds to the case that waves are propagating along the $+z$ axis.

four quasidegenerate eigenstates are supported in the latter subspace. This phenomenon is different from the previous results by encircling EPs in a non-Hermitian system possessing only one lowest-loss eigenvalue sheet, where the output state is composed of only one eigenstate [22–28,52]. Our system possesses four quasidegenerate lowest-loss eigenvalue sheets and as a result, the encircling outcomes are superposition states that consist of all the four lowest-loss eigenmodes.

The above phenomenon is related to the NATs that occurred in the encircling process [21,50,55]. For a more in-depth understanding of the mechanism, we demonstrate the detailed physics associated with the NATs. We can solve the Schrödinger-like equation to obtain the evolution of the state vector $|\phi(z)\rangle$ during the whole period of evolution. This means that there are eight instantaneous eigenvectors that can be projected onto the instantaneous state vector $|\phi(z)\rangle$ at any position on the z axis. The one with the largest amplitude among the eight coefficients is selected as that of the dominant instantaneous eigenstate. We extract the real part of the eigenvalue of the dominant instantaneous eigenstate and plot them in Fig. 4(a), when the eigenmodes 1–4 are used as the

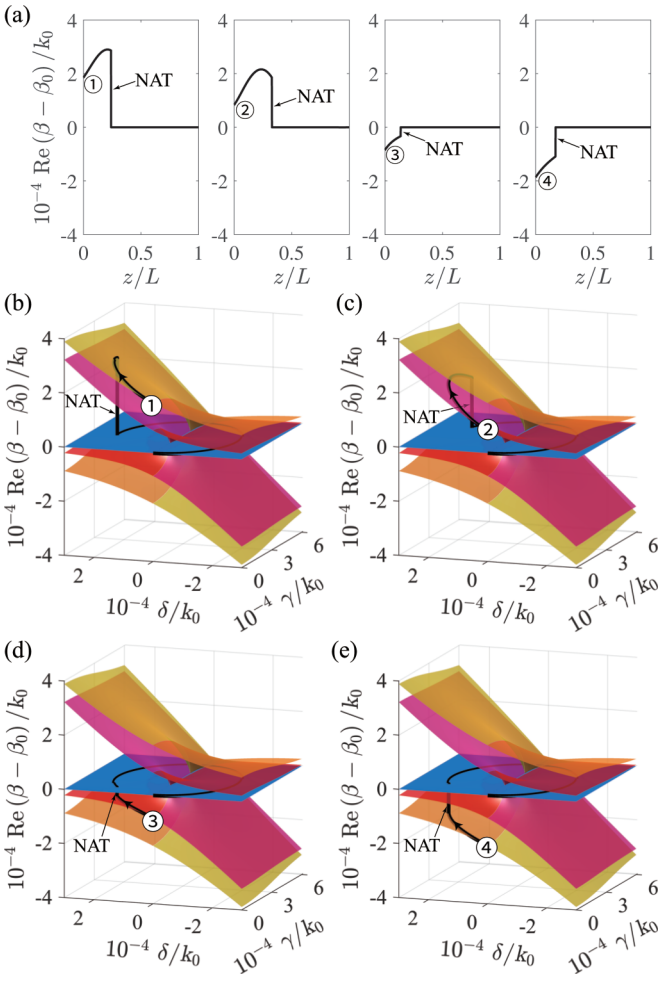

FIG. 4. (a) Calculated real part of the eigenvalue of the dominant eigenstate in the evolution process where two EPs are dynamically encircling in a CW direction, with eigenmodes 1, 2, 3 and 4 being the initial condition. (b)–(e) The exacted trajectory of the dominant eigenstate on the energy sheets with mode 1 (b), mode 2 (c), mode 3 (d) and mode 4 (e) being the initial state. Each initial state undergoes a NAT process and evolves to be a superposition of the four quasidegenerate states exhibiting the lowest loss eventually.

initial state (from left to right). We find that after a particular evolutionary length, each value will abruptly drop to zero (i.e., $\beta = \beta_0$), indicating the emergence of NATs from a higher-loss state to a lower-loss one. The NAT process is irreversible so that the states are stable when it evolves on the lowest-loss eigenvalue sheet (i.e., the blue sheet). These NAT processes finally result in the linear combination of the four lowest-loss eigenstates as the output. In Figs. 4(b)–4(e), we also label the results for the four cases separately on the real part eigenvalue sheets, which can demonstrate the trajectories of the dominant eigenstate in our CW-loop device. Regardless of the input, the results clearly suggest that the final state is on the lowest-loss degenerate sheet.

We also change the direction to encircle the EPs (i.e., looping in a CCW trajectory) and repeat the calculation of Fig. 3. The results are given in Fig. 5 where the input states are as same as the former. We present these results in the opposite arrangement in order to distinguish them from the

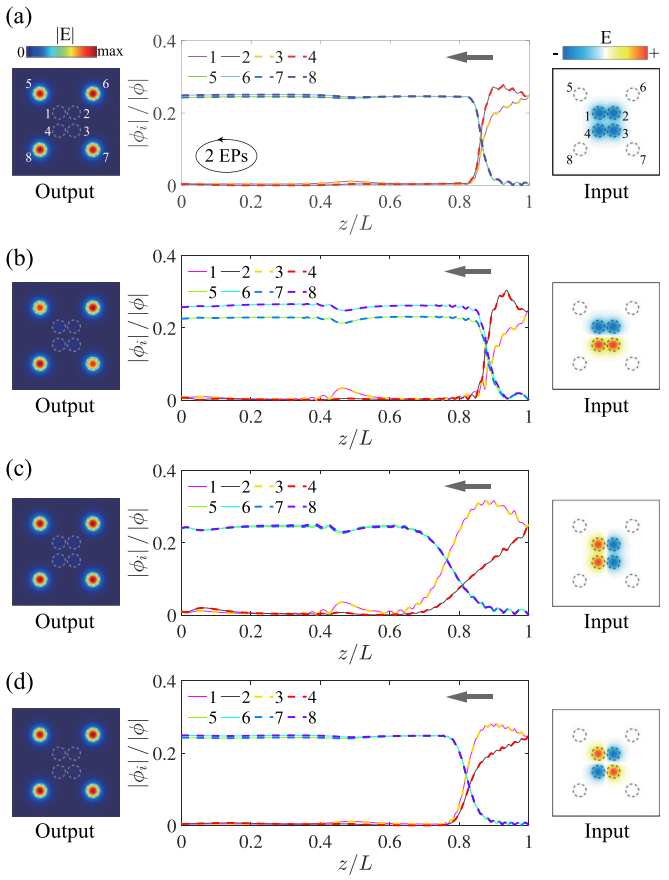

FIG. 5. Numerically simulated evolution of the normalized components of $|\phi(z)\rangle$ with eigenmodes 1 (a), 2 (b), 3 (c), and 4 (d) being the initial state. All conditions are the same as those in Fig. 3 except for a CCW loop direction, corresponding to wave transmissions along the -z axis.

CW loop case. Comparing the two situations with each other, we can observe similar phenomenon that during either CW or CCW loops, the final state is always a superposition state that is composed of the four lowest-loss eigenmodes and the NAT occurs merely once in the evolution process. We state that the crossing of the calculated coefficients in the middle panel of Figs. 3 and 5 is also a hallmark of the NAT. The results in CW and CCW loops indicate that encircling the two EPs in our structure exhibits a nonchiral feature for switching eigenstates. As a result, one cannot discriminate the encircling direction by simply measuring the final state in our system, which is in stark contrast to the system with only one lowest-loss sheet [21–28,52], where the chiral dynamics allows one to distinguish the encircling direction simply via the measurement of the final state.

III. ROBUSTNESS OF THE DYNAMICS

One might ask whether these calculations are under adiabatic conditions in the presence of NATs, which means that the "time scale" of evolution (i.e., the length of the waveguide) should be large enough. In fact, the adiabatic theorem is indeed a prerequisite for observing EP encirclement induced dynamics [51,56]. The system we study already satisfies the

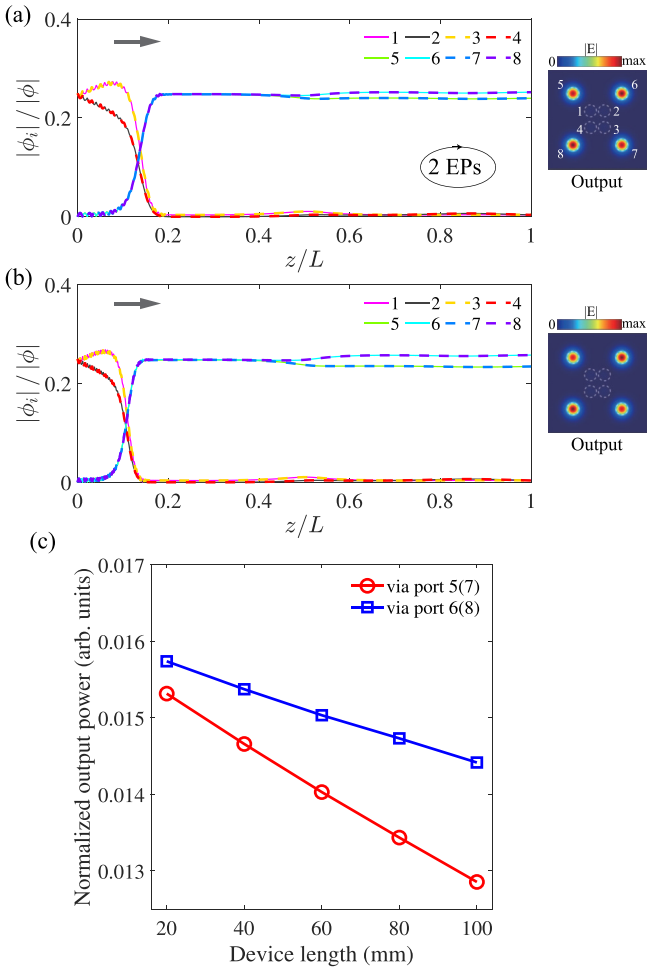

FIG. 6. Calculated ratio of the components of $|\phi(z)\rangle$ when the EPs are encircled in a CW loop with mode 1 being the initial state, where the device length is (a) $L = 400$ mm, (b) $L = 800$ mm. The right panel shows the output field patterns. (c) Calculated output power at waveguides 5(or 7) and 6(or 8) as a function of the device length when excited by mode 1.

adiabatic condition in terms of the length selection. This can be verified by the fact that a similar phenomenon can be observed when the length of the waveguide is increased. To throw light on this opinion further, we repeat the calculation in the device analyzed in Fig. 3(a) (i.e., the dynamical encircling in a CW loop when eigenmode 1 is used as the input) but choose a different device length. The results with $L = 400$ mm and $L = 800$ mm are shown in Figs. 6(a) and 6(b), respectively. Compared with Fig. 3(a), we find that under different lengths the phenomena are the same, i.e., the fields in edge waveguides rapidly outgrow due to NATs, while those of the inner waveguides 1 to 4 decline to zero. However, with the increase in the waveguide length, the NAT will appear at a shorter relative position of the system z/L. This reveals the so-called topological robustness of non-Hermitian systems in the existence of NATs, which is quite different from that in Hermitian systems as the phenomenon here is robust and independent of the device length. We also calculate the output power at waveguides 5 (or 7) and 6 (or 8) for lengths from 200 to 1000 mm by assuming the input power is in normalized

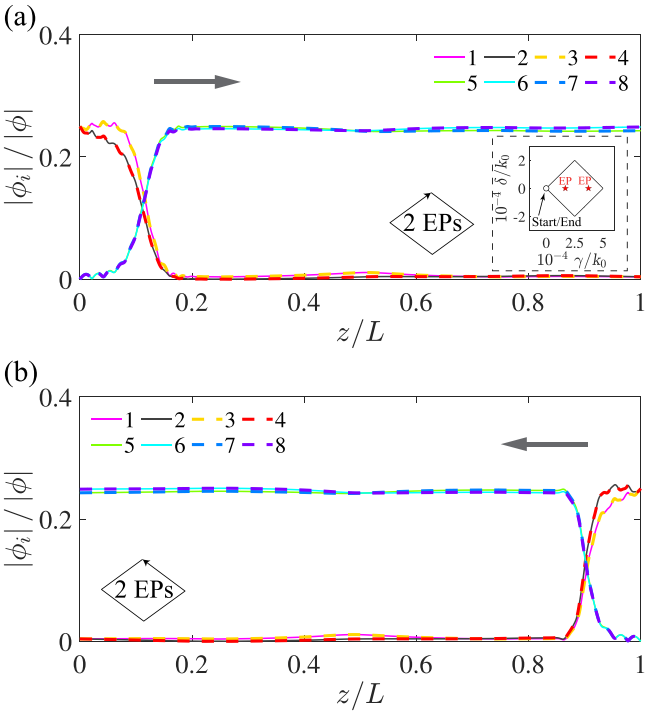

FIG. 7. Calculated ratio of the components of $|\phi(z)\rangle$ with a rhombus CW loop (a) and CCW loop (b) in the parameter space. The initial state is mode 1. The inset of (a) shows the exacted position of the two EPs and the rhombus encircling loop.

unit. The results are plotted in Fig. 3(c), which is used to clarify the above robustness. Obviously, non-Hermitian systems possess losses, therefore the output power decays with increasing waveguide length. Despite this, the output powers are still distributed in the four edge waveguides, which clearly demonstrates the robustness of the discovered phenomenon by dynamically encircling EPs in non-Hermitian systems with quasidegenerate energy levels.

The discovered phenomenon is also robust to the form of the trajectories around the EPs. Let us consider a rhombus encircling loop in the parameter space [see the inset of Fig. 7(a)] rather than the elliptical loop before. The starting point of the rhombus is the same as the previous configuration, and the coordinates of the other three vertices (on the $\delta-\gamma$ axis) are $(5\times10^{-4}k_0, 0)$ and $(2.5\times10^{-4}k_0, \pm2\times10^{-4}k_0)$ to ensure that both EPs are enclosed. We repeat the circumstances in Figs. 3(a) and 5(a) and recalculate the mode evolution with the results given in Figs. 7(a) (CW loop) and 7(b) (CCW loop). Since the robust dynamics is protected by the topological structure surrounding the EPs, the exact form of the loop does not affect the dynamics as long as the EPs are enclosed. The results show nothing unique compared to the elliptical loop, except that the NAT occurs at shorter distances, which manifests the topological robustness to the encircling loop.

IV. DISCUSSION

Finally, we discuss the difference between the chiral behavior brought by EP encirclement in non-Hermitian systems with only one lowest-loss energy level [22–28] and the

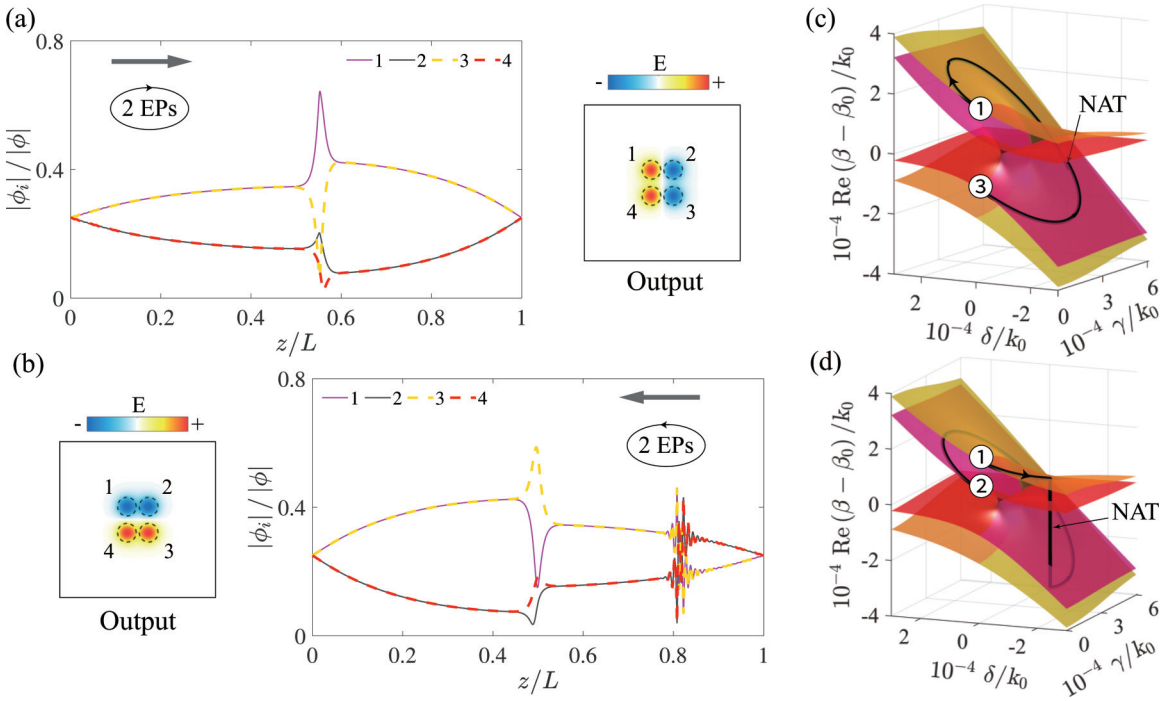

FIG. 8. A system for comparison where the edge waveguides are removed so that only one lowest-loss sheet exists. (a) and (b) The evolution of the components of $|\phi(z)\rangle$ in the EP-encirclement process in a CW (a) and CCW direction (b). (c) and (d) The trajectory of the dominant eigenstate on the energy sheets, corresponding to the processes in (a) and (b), respectively.

nonchiral feature found in our system with multiple quasidegenerate energy levels. We build a new system for comparison by simply removing the edge waveguides 5–8, in which only the four eigenstates with defined nonzero losses in the previous configuration are left. The Hamiltonian then degenerates to a 4×4 matrix and exhibits only one lowest-loss eigenstate instead of the four mentioned above. We apply the same method to explore the evolutionary chirality of this system in both CW and CCW loops. We select the first eigenmode (which is nearly the same as the previous defined eigenmode 1 in the eight-waveguide system) as input to demonstrate the evolution of field and output field distribution [see Figs. 8(a) and 8(b)] for both encircling directions. The dominant eigenvector projection of the corresponding process is also given in Figs. 8(c) and 8(d). We find that the eigenmode 1 from the upper sheet always shifts to lowest-loss one represented by the magenta sheet in Figs. 8(c) and 8(d) after going through NAT once. The same dynamics can also be found when the initial state is the eigenmode 2–4 (the results are not shown here). The output state is found to be independent of the input, but is solely determined by the encircling direction. The output of the CW loop is always the eigenmode 3, while that of the CCW loop is the eigenmode 2. In this consideration, a starting point at the $\mathcal{PT}$-symmetric phase where the eigenstates of the system share the same lowest-loss bifurcating on both sides of the eigenvalue topology space can account for the chiral dynamics [22,24–26,51]. Although the starting point in the eight-waveguide system is also located at this "$\mathcal{PT}$-symmetric phase", the four edge waveguides enable the support of four quasidegenerate states with even lower losses, which then can be regarded as the new target of the NATs. Since the quasidegenerate eigenvalue sheets do not possess the bifurcation topology, the dynamics by encircling the two EPs is nonchiral, which is completely different from the phenomenon in conventional EP-encirclement systems. We also discuss the "time step" at which the NAT occurs in devices with different lengths. Without loss of generality, we consider the CW-loop device with eigenmode 1 being the input. We calculate the relative position of NAT (i.e., z/L) as a function of the device length in Fig. 9(a) and the corresponding location in the $\delta-\gamma$ parameter space is also marked in Fig. 9(b). We find that the NAT occurs at an "earlier time" when increasing the device length. The phenomenon can be attributed to the fact that the NAT requires that the state experiences losses for some time on the higher-loss energy sheet. When the length of device is longer, experiencing the same loss will make the relative position decrease.

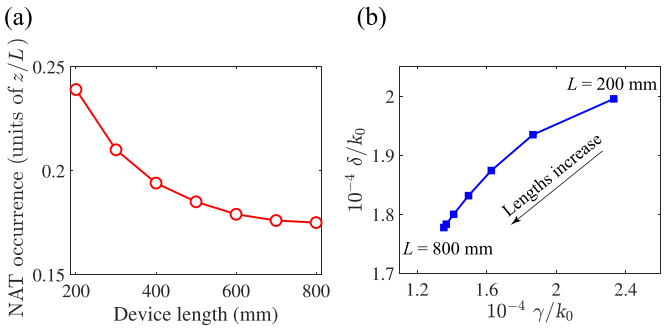

FIG. 9. (a) The calculated relative position of the NAT as a function of the device length L. (b) The position of NAT in the $\delta-\gamma$ parameter space for different L.

V. CONCLUSION

In summary, we have theoretically investigated the physics in the process of dynamically encircling EPs in a non-Hermitian system with quasidegenerate lowest-loss eigenvalue sheets. We found a nonchiral behavior of switching eigenstates, where the final state is a superposition of multiple quasidegenerate states. This is in stark contrast to the previous chiral dynamics found in the EP-encircling process where the output is a single mode. The phenomenon is protected by the multiple quasidegenerate eigenvalue sheets, and as a result, it is robust to a certain disturbance of the system parameters including the device length and the exact form of the loop. Our work has extended the understanding in the EP-encirclement process from another perspective and may provide new ways to manipulate waves in non-Hermitian systems.

ACKNOWLEDGMENT

This work was supported by the National Natural Science Foundation of China (Grant No. 11974140).

[1] T. Kato, *Perturbation Theory for Linear Operators* (Springer, New York, 1966).
[2] M. V. Berry, Czech. J. Phys. **54**, 1039 (2004).
[3] N. Moiseyev, *Non-Hermitian quantum mechanics* (Cambridge University Press, New York, 2011).
[4] W. D. Heiss, J. Phys. A **45**, 444016 (2012).
[5] R. El-Ganainy, K. G. Makris, M. Khajavikhan, Z. H. Musslimani, S. Rotter, and D. N. Christodoulides, Nat. Phys. **14**, 11 (2018).
[6] D. Zhang, X. Q. Luo, Y. P. Wang, T. F. Li, and J. Q. You, Nat. Commun. **8**, 1368 (2017).
[7] X. Zhang, K. Ding, X. Zhou, J. Xu, and D. Jin, Phys. Rev. Lett. **123**, 237202 (2019).
[8] T. X. Lu, H. Zhang, Q. Zhang, and H. Jing, Phys. Rev. A **103**, 063708 (2021).
[9] K. Ding, G. Ma, M. Xiao, Z. Q. Zhang, and C. T. Chan, Phys. Rev. X **6**, 021007 (2016).
[10] W. Tang, X. Jiang, K. Ding, Y. X. Xiao, Z. Q. Zhang, C. T. Chan, and G. Ma, Science **370**, 1077 (2020).
[11] C. Shi, M. Dubois, Y. Chen, L. Cheng, H. Ramezani, Y. Wang, and X. Zhang, Nat. Commun. **7**, 11110 (2016).
[12] Y. Choi, S. Kang, S. Lim, W. Kim, J.-R. Kim, J. H. Lee, and K. An, Phys. Rev. Lett. **104**, 153601 (2010).
[13] B. Peng, Ş. K. Özdemir, S. Rotter, H. Yilmaz, M. Liertzer, F. Monifi, C. M. Bender, F. Nori, and L. Yang, Science **346**, 328 (2014).
[14] H. Jing, Ş. K. Özdemir, Z. Geng, J. Zhang, X. Y. Lü, B. Peng, L. Yang, and F. Nori, Sci. Rep. **5**, 9663 (2015).
[15] Z. P. Liu, J. Zhang, Ş. K. Özdemir, B. Peng, H. Jing, X. Y. Lü, C. W. Li, L. Yang, F. Nori, and Y. X. Liu, Phys. Rev. Lett. **117**, 110802 (2016).
[16] B. Peng, Ş. K. Özdemir, M. Liertzer, W. Chen, J. Kramer, H. Yilmaz, J. Wiersig, S. Rotter, and L. Yang, Proc. Natl. Acad. Sci. USA. **113**, 6845 (2016).
[17] H. Xu, D. Mason, L. Jiang, and J. G. E. Harris, Nature (London) **537**, 80 (2016).
[18] W. Chen, Ş. K. Özdemir, G. Zhao, J. Wiersig, and L. Yang, Nature (London) **548**, 192 (2017).
[19] H. Lü, C. Wang, L. Yang, and H. Jing, Phys. Rev. Appl. **10**, 014006 (2018).
[20] J. Zhang, B. Peng, Ş. K. Özdemir, K. Pichler, D. O. Krimer, G. Zhao, F. Nori, Y. Liu, S. Rotter, and L. Yang, Nat. Photonics **12**, 479 (2018).
[21] J. Doppler, A. A. Mailybaev, J. Böhm, U. Kuhl, A. Girschik, F. Libisch, T. J. Milburn, P. Rabl, N. Moiseyev, and S. Rotter, Nature (London) **537**, 76 (2016).
[22] J. W. Yoon, Y. Choi, C. Hahn, G. Kim, S. H. Song, K.-Y. Yang, J. Y. Lee, Y. Kim, C. S. Lee, J. K. Shin, H.-S. Lee, and P. Berini, Nature (London) **562**, 86 (2018).
[23] X.-L. Zhang, S. Wang, B. Hou, and C. T. Chan, Phys. Rev. X **8**, 021066 (2018).
[24] X.-L. Zhang, T. Jiang, and C. T. Chan, Light: Sci. Appl. **8**, 88 (2019).
[25] X.-L. Zhang and C. T. Chan, Commun. Phys. **2**, 63 (2019).
[26] A. Li, J. Dong, J. Wang, Z. Cheng, J. S. Ho, D. Zhang, J. Wen, X.-L. Zhang, C. T. Chan, A. Alù, C.-W. Qiu, and L. Chen, Phys. Rev. Lett. **125**, 187403 (2020).
[27] S.-R. Yang, X.-L. Zhang, and H.-B. Sun, Exploration **2**, 20210243 (2022).
[28] F. Yu, X.-L. Zhang, Z.-N. Tian, Q.-D. Chen, and H.-B. Sun, Phys. Rev. Lett. **127**, 253901 (2021).
[29] Y. Meng, Y. Chen, L. Lu, Y. Ding, A. Cusano, J. A. Fan, Q. Hu, K. Wang, Z. Xie, Z. Liu, Y. Yang, Q. Liu, M. Gong, Q. Xiao, S. Sun, M. Zhang, X. Yuan, and X. Ni, Light: Sci. Appl. **10**, 235 (2021).
[30] M. Zhang, W. Sweeney, C. W. Hsu, L. Yang, A. D. Stone, and L. Jiang, Phys. Rev. Lett. **123**, 180501 (2019).
[31] J. Chen, Y. Wang, T. Fu, X. Wang, Y. Dai, and W. Zheng, Appl. Phys. Express **14**, 122005 (2021).
[32] B. Midya, H. Zhao, and L. Feng, Nat. Commun. **9**, 2674 (2018).
[33] L. Xiao, T. Deng, K. Wang, G. Zhu, Z. Wang, W. Yi, and P. Xue, Nat. Phys. **16**, 761 (2020).
[34] M. Parto, Y. G. N. Liu, B. Bahari, M. Khajavikhan, and D. N. Christodoulides, Nanophotonics **10**, 403 (2020).
[35] W. Wang, W. Gao, L. Cao, Y. Xiang, and S. Zhang, Light: Sci. Appl. **9**, 40 (2020).
[36] Z. Chen and M. Segev, Elight **1**, 2 (2021).
[37] Z. Lin, H. Ramezani, T. Eichelkraut, T. Kottos, H. Cao, and D. N. Christodoulides, Phys. Rev. Lett. **106**, 213901 (2011).
[38] X. Yin and X. Zhang, Nat. Mater. **12**, 175 (2013).
[39] Y. Huang, Y. Shen, C. Min, S. Fan, and G. Veronis, Nanophotonics **6**, 977 (2017).
[40] X. Huang, C. Lu, C. Liang, H. Tao, and Y.-C. Liu, Light: Sci. Appl. **10**, 30 (2021).
[41] C. Wang, X. Jiang, G. Zhao, M. Zhang, C. W. Hsu, B. Peng, A. D. Stone, L. Jiang, and L. Yang, Nat. Phys. **16**, 334 (2020).
[42] C. Wang, X. Jiang, W. R. Sweeney, C. W. Hsu, Y. Liu, G. Zhao, B. Peng, M. Zhang, L. Jiang, A. Douglas Stone, and L. Yang, Proc. Natl. Acad. Sci. USA **118**, e2012982118 (2021).

[43] Y. Sun, W. Tan, H. Q. Li, J. Li, and H. Chen, Phys. Rev. Lett. **112**, 143903 (2014).
[44] Q. Zhong, R. El-Ganainy, S. Nelson, and Ş. K. Özdemir, Opt. Lett. **44**, 5242 (2019).
[45] W. R. Sweeney, C. W. Hsu, S. Rotter, and A. D. Stone, Phys. Rev. Lett. **122**, 093901 (2019).
[46] C. Wang, W. R. Sweeney, A. D. Stone, and L. Yang, Science **373**, 1261 (2021).
[47] H. Hodaei, M. A. Miri, M. Heinrich, D. N. Christodoulides, and M. Khajavikhan, Science **346**, 975 (2014).
[48] J. B. Khurgin, Optica **7**, 1015 (2020).
[49] L. Li, Y. Cao, Y. Zhi, J. Zhang, Y. Zou, X. Feng, B.-O. Guan, and J. Yao, Light: Sci. Appl. **9**, 169 (2020).
[50] I. Gilary, A. A. Mailybaev, and N. Moiseyev, Phys. Rev. A **88**, 010102(R) (2013).
[51] T. J. Milburn, J. Doppler, C. A. Holmes, S. Portolan, S. Rotter, and P. Rabl, Phys. Rev. A **92**, 052124 (2015).
[52] W. Liu, Y. Wu, C.-K. Duan, X. Rong, and J. Du, Phys. Rev. Lett. **126**, 170506 (2021).
[53] A. Laha, S. Dey, H. K. Gandhi, A. Biswas, and S. Ghosh, ACS Photonics **7**, 967 (2020).
[54] S. Dey, A. Laha, and S. Ghosh, Phys. Rev. B **101**, 125432 (2020).
[55] M. V. Berry and R. Uzdin, J. Phys. A **44**, 435303 (2011).
[56] R. Uzdin, A. Mailybaev, and N. Moiseyev, J. Phys. A **44**, 435302 (2011).
[57] X.-Q. Liu, Y.-L. Zhang, Q.-K. Li, J.-X. Zheng, Y.-M. Lu, S. Juodkazis, Q.-D. Chen, and H.-B. Sun, PhotoniX **3**, 1 (2022).
[58] X.-L. Zhang, F. Yu, Z.-G. Chen, Z.-N. Tian, Q.-D. Chen, H.-B. Sun, and G. Ma, Nat. Photon. **16**, 390 (2022).